Journal of Catalysis 432 (2024) 115363

Contents lists available at ScienceDirect

Journal of Catalysis

journal homepage: www.elsevier.com/locate/jcat

Research article

Theoretical investigation of the paring mechanism of the MTO process in different zeolites

Annika E. Enss [a], Philipp N. Plessow [a], Felix Studt [a,b,*]

[a] Karlsruhe Institute of Technology, Institute of Catalysis Research and Technology, Hermann-von-Helmholtz-Platz 1, Eggenstein-Leopoldshafen, 76344, Germany
[b] Karlsruhe Institute of Technology, Institute for Technical Chemistry and Polymer Chemistry, Engesserstr. 18 / 20, Karlsruhe, 76131, Germany

ARTICLE INFO

Keywords:
Methanol-to-olefins
Aromatic-based cycle
Hydrocarbon pool
Zeolite catalysis
Density functional theory

ABSTRACT

The paring mechanism, which belongs to the aromatic cycle of the methanol-to-olefins process and produces propene, is investigated for H-ZSM-5 (MFI structure), H-SSZ-24 (AFI structure) and H-SAPO-34 (CHA structure) with the heptamethylbenzylium cation as a co-catalyst using DFT and ab initio calculations. We focus on the mechanistic pathway of the paring mechanism that we have proposed recently for H-SSZ-13 [Catal. Sci. Technol. 12 (2022) 3516–3523.], in which ring contraction occurs from hexamethylmethylenecyclohexadiene and the resulting five-membered ring keeps an unsaturated methylene group throughout the process, leading to tetramethylfulvene as the intermediate after propene elimination. The highest free energy barriers (at 400 °C) for this mechanism are found to be 139 kJ/mol, 156 kJ/mol and 167 kJ/mol for H-SAPO-34, H-SSZ-24 and H-ZSM-5, respectively, compared to 127 kJ/mol for H-SSZ-13. All these barriers are low enough to be kinetically relevant and can thus explain the observed formation of propene as one of the main products of the MTO-process in these zeolites. The barriers for polymethylbenzene methylation to recover the active species are higher than the barriers for the paring mechanism in all zeolites (164 kJ/mol, 187 kJ/mol and 189 kJ/mol for H-SAPO-34, H-SSZ-24 and H-ZSM-5, compared to 163 kJ/mol for H-SSZ-13). The lowest barriers are found for H-SAPO-34, which is often the commercial catalyst in methanol-to-propene plants.

1. Introduction

Zeolite catalysts are vividly debated in the chemical industry as catalysts for sustainable carbon–neutral processes as they can facilitate the methanol-to-olefins (MTO) process, which can use renewably produced methanol (MeOH) to produce hydrocarbon products. [1–6] The MTO process comprises a complex reaction network, which has been subject of both experimental [4,7–13] and theoretical [4,7,14–22] studies. These studies established the concept of the so-called hydrocarbon pool (HCP) originally developed by Dahl and Kolboe. [23–25] It divides the co-catalytic reaction within the zeolite pores into two subcycles: The olefin cycle that produces olefins by repeated methylation and cracking of already produced olefins. The other is the aromatic cycle. Here, olefins are produced either by methylation and elimination of the aromatic side chains (side-chain mechanism) or by ring contraction and expansion, producing a propene side chain which can be eliminated. Until recently, the paring pathway was proposed to proceed via contraction of the heptamethylbenzenium cation (heptaMB$^+$), eliminating propene from a positively charged propylgroup with an antiaromatic intermediate following suggestions from Sullivan et al. dating back to the 1960s. [26] The reaction barriers of this mechanism have been computed to be 240 kJ/mol or higher in H-ZSM-5 and H-SAPO-34 [14,15], which are the two commercially employed catalysts. [27] These rather high barriers lead Wang et al. to conclude, that the paring mechanism is not a feasible reaction pathway. Another study from Chen et al. for H-ZSM-22, H-BEA, H-ZSM-5 and H-SAPO-34 also found barriers for the paring mechanism, that were 200 kJ/mol or higher for all investigated zeolites. [28] In contrast, an experimental study from Olsbye and co-workers [29], investigating the dealkylation of heptaMB$^+$, showed evidence that the paring, rather than the side chain mechanism, was the dominant reaction pathway in H-SSZ-24 (AFI structure). In this study heptaMB$^+$ with ^{13}C-labelled ring carbons was introduced, leading to one or two ring carbons to be incorporated into the product species. Isotope labelling was also used by Hwang et al., who showed that also in H-SAPO-34, propene is produced from hexamethylbenzene via the paring mechanism. [30]

In a recent paper from our group using H-SSZ-13 [31], we proposed an alternative paring mechanism (Fig. 1), which does not include

* Corresponding author.
E-mail address: felix.studt@kit.edu (F. Studt).

https://doi.org/10.1016/j.jcat.2024.115363
Received 26 October 2023; Received in revised form 10 January 2024; Accepted 7 February 2024
Available online 10 February 2024

antiaromatic intermediates. In this mechanism, propene is eliminated from a neutral propyl group with the positive charge located in the 5-membered ring, so that after elimination tetramethylfulvene remains as a neutral intermediate. For H-SSZ-13 the highest free energy barrier (at 400 °C) to be overcome was 142 kJ/mol, rendering this pathway kinetically relevant.

Herein, we study this new paring mechanism for H-ZSM-5, H-SAPO-34 and H-SSZ-24 using DFT and ab initio calculations, in order to investigate the impact of zeolite topology and acidity on this mechanism for the most relevant zeotypes. H-ZSM-5 with MFI structure and H-SAPO-34 with CHA structure were chosen for their industrial relevance. [27] H-SSZ-24 (AFI structure) was used as a comparison to the experimental study of Olsbye and co-workers [29] and to investigate the difference of a system with larger, one-dimensional pores to the three-dimensional pore network of MFI and the cage structure of CHA.

2. Computational details

Structure optimizations were performed using periodic DFT with the dispersion-corrected PBE-D3[32,33] functional, a convergence criterion of 0.001 eV/Å and *k*-point sampling only at the Γ-point. The Vienna Ab Initio Simulation Package [34] (VASP) version 5.4.1 using the atomic simulation environment [35] (ASE) with the projector-augmented wave method (PAW) and an energy cutoff of 400 eV was used to carry out calculations.

The unit cell of the H-SAPO-34 model contains 36 T-atoms, which are alternating aluminum and phosphor atoms, with one phosphor atom exchanged by a silicon atom. The optimized lattice parameters of the unit cell are a = 13.875, b = 13.875 and c = 15.017 Å, as used in previous work. [36] The CHA structure of H-SAPO-34 consists of cavities formed by a double 6-membered ring connected by 8-membered ring windows. The effective diameter of the cavity is 10.8 Å, whereas the diameter of the 6-membered ring is only 6.2 Å. [37] The H-ZSM-5 model has a unit cell of the MFI structure with lattice parameters a = 20.34, b

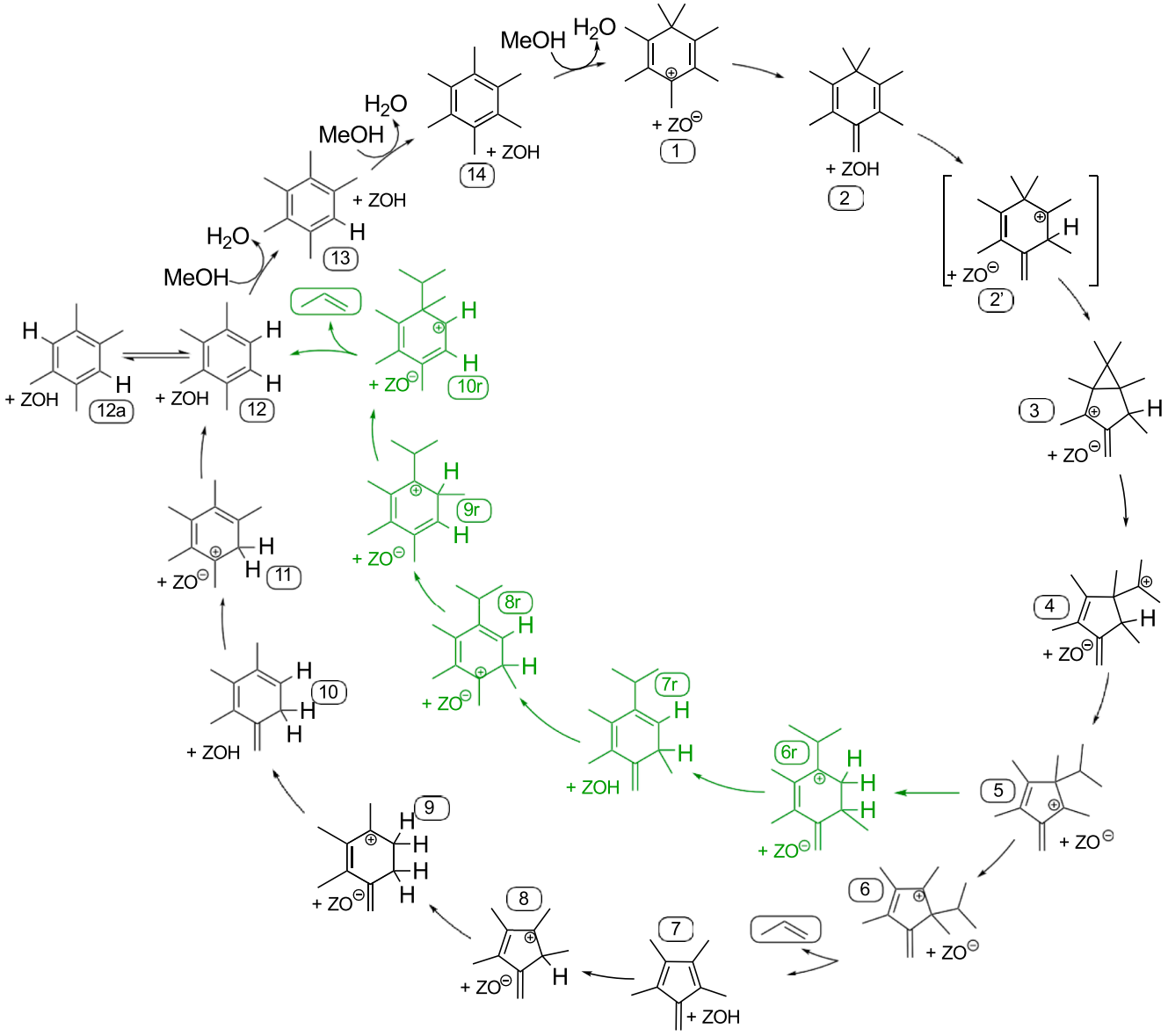

Fig. 1. Mechanistic overview of the paring mechanism investigated in this paper. The outer black pathway shows the detailed paring mechanism as introduced in our previous paper [31], with propene elimination taking place before ring expansion. Shown in green is a variant of the paring mechanism in which the ring is expanded again before propene is eliminated, this was also proposed previously. [31]. (For interpretation of the references to color in this figure legend, the reader is referred to the web version of this article.)

= 19.988 and c = 13.492 Å as optimized in previous work. [36] The T12 site, which is typically used in theoretical studies [38–40], was chosen as acid site location. The unit cell therefore has a Si/Al ratio of 95. The MFI structure is formed by two channel systems, a straight and a sinusoidal channel, both formed by 10-membered rings. The pore diameter in H-ZSM-5 is 8.7 Å. [37] For H-SSZ-24, optimized lattice parameters from previous work [37] are a = 13.886, b = 13.886 and c = 8.606 Å. To avoid interactions of close acid sites, a supercell containing two unit cells in the direction of lattice parameter c were used in our calculations, thus creating an AFI cell with a Si/Al ratio of 47. [37] The AFI structure is given by a one-dimensional pore system of 12-membered rings with a pore diameter of 11.3 Å.[37]

For vibrational analysis, a partial Hessian was calculated including the substrate atoms and the acid site, consisting of the aluminum atom and all adjacent oxygen and silicon atoms. Gibbs free energies were calculated using the harmonic-oscillator, rigid-rotator and free-translator approximations. Since low vibrational frequencies lead to large entropic inaccuracies in the harmonic-oscillator approximation [41,42], frequencies with less than 12 cm^{-1} were raised to that value. Transition states were generally calculated with automated relaxed potential energy surface scans [43] (ARPESS) and in some cases also with the nudged elastic band [44] (NEB) and the dimer method. [45] To confirm the connectivity of transition states, structures were distorted along the direction of the transition mode and subsequently optimized towards the endpoints. DFT calculations usually underestimate transition state energies, e.g. by up to 50 kJ/mol in the case of PBE-D3. [46,47] We therefore calculated clusters including active site and reactant with higher-level methods similar to approaches developed by Sauer and co-workers. [48–51] The resulting energy correction is added to the DFT energies: [52].

$$\Delta E^{cluster} = E^{cluster}_{MP2/CBS} + \Delta E^{cluster}_{\Delta CCSD(T)/DZ} - \Delta E^{cluster}_{PBE-D3} \quad (1)$$

Here, we use complete basis set (CBS) extrapolated Møller- Plesset second order perturbation theory (MP2) calculations to compute $E^{cluster}$. [53] This includes Hartree-Fock (HF) and MP2 correlation separately extrapolated with cc-pVDZ, cc-pVTZ and cc-pVQZ basis sets using three-point exponential fit [54] and cc-pVDZ and cc-pVTZ using the two-point X^{-3} fit [55], respectively. For HF, MP2 and CCSD(T) calculations, the ORCA program package (version 4.2.1) was used. [56] The basis sets used were cc-pVDZ and cc-pVXZ [57] with X = D,T for CCSD(T) and MP2, respectively. The difference between CCSD(T) and MP2 was evaluated using DLPNO-CCSD(T) [58–60] with the cc-pVDZ basis set, which was proven to be reliable in a previous benchmark study. [46] We evaluated this methodology for the reaction of methanol to propene and water in section S6 in the SI. The DLPNO approximation uses the'-TightPNO' threshold. [60–62] HF calculations were performed with basis sets cc-pVXZ with X = D,T,Q and the RIJCOSX approximation [63] with GridX6. VASP version 5.4.1 was used to carry out DFT calculations on cluster models, using the PBE-D3 functional.

Cluster models of H-ZSM-5, H-SAPO-34 and H-SSZ-24 contain 44, 46 and 66 T-sites, respectively. Microkinetic modelling was performed with the surfprobe program of the DETCHEM software package [64] at a reference pressure of 1 bar MeOH. Coverages and fluxes were evaluated after 10^4 s to ensure convergence to steady states. With a surface coverage of 1 mol / cm^2, turnover frequencies (TOFs) were calculated from the propene surface fluxes.

3. Results and discussion

The paring mechanism (Fig. 1) is usually discussed using poly-methylbenzenes as the aromatic co-catalyst. Since methylation of benzene from either MeOH or dimethyl ether (DME) is thermodynamically favored, poly-methylated benzenes such as hexa- and pentamethylbenzene are commonly discussed as the acting co-catalyst. [65] For simplicity, due to its high symmetry, we only consider hexamethylbenzene (hexaMB, structure 14) in this study. Methylation of hexaMB yields the heptamethylbenzenium cation (heptaMB$^+$, structure 1), which is usually employed as the reference point, as this is typically more stable than the neutral hexaMB, in our case by 15 kJ/mol for H-SSZ-13[31], 7 kJ/mol for H-ZSM-5 and 40 kJ/mol for H-SSZ-24. However, for H-SAPO-34, hexaMB and heptaMB$^+$ are similar in stability at 400 °C, differing by 1 kJ/mol in Gibbs free energy (see Fig. 2 a)).

There are two variants of the revised paring mechanism [31], which are both shown in Fig. 1. Propene elimination can occur from the five-membered ring (black pathway), followed by ring-expansion to a six-membered ring. Alternatively, ringexpansion can happen first (green pathway) and propene is eliminated from the six-membered ring. We will first discuss propene elimination from the five-membered ring, where the computed Gibbs free energies are shown in Fig. 2. Starting from structure 1 (heptaMB$^+$), the methyl group in *para*-position to the ring carbon substituted by two methyl groups is first deprotonated to form hexamethylmethylenecyclohexadiene (HMMC, structure 2). Ring contraction to a five-membered ring with a fused three-membered ring (structure 3) occurs upon HMMC protonation in the *ortho*-position relative to the methylene group. This reaction proceeds through the structure labeled 2′, which is simply a protonated six-membered ring. However, for all catalysts except H-ZSM-5, structure 2′ is actually not a minimum and protonation of HMMC (structure 2) leads in these cases directly to structure 3 via TS(2–3). For H-ZSM-5, we found a transition state (TS(1-2′)) that leads through deprotonation and re-protonation in one step from heptaMB$^+$ (structure 1) to structure 2′. Therefore, the values shown in Fig. 2 for TS(1–2) and TS(2–3) for H-SAPO-34 and H-SSZ-24 correspond to TS(1-2′) and TS(2′-3) for H-ZSM-5.

The fused three-membered ring opens to give structure 4, in which a positive charge is located on the isopropyl group. The charge is shifted to the five-membered ring during a hydride transfer from a ring-carbon to the isopropyl group (structure 5). From structure 5, the isopropyl group shifts along the ring, and is subsequently eliminated from structure 6. In the elimination step, the isopropyl cation protonates the active site to give propene and the neutral tetramethylfulvene (structure 7). In this pathway of the paring mechanism (black pathway in Fig. 1), propene-elimination through TS(6–7) is the highest reaction barrier for three of the four investigated zeolites (H- SSZ-13,[31] H-ZSM-5 and H-SAPO-34), with a very similar transition state structure as shown in Fig. 2 b)-e).

After protonation of tetramethylfulvene to structure 8, ring expansion to a six-membered ring takes place. Here, the methyl group at the doubly substituted ring carbon inserts into the C–C bond to the adjacent carbon, concertedly donating one of its hydrogen atoms to the ring, yielding the six-membered ring structure 9. In this pathway (black in Fig. 1), this step is the highest reaction barrier for H-SSZ-24. After several protonation and deprotonation steps, 1,2,3,4-tetramethylbenzene (structure 12) is formed. To close the catalytic cycle, two methylation steps are needed to form hexamethylbenzene, and a third methylation to reach the heptamethylbenzenium cation. These can occur by directly reacting with MeOH or by reacting with a surface-methoxy-species (SMS). PentaMB can also not only be methylated directly at the ring-carbon without a methylgroup, but in a geminal way, followed by methylshifts and finally deprotonation of hexaMB$^+$. In case of H-SAPO-34, isomerization of 1,2,3,4-tetramethylbenzene to 1,2,4,5-tetramethylbenzene (structure 12a) leads to a lower methylation barrier than direct methylation of 12. All these methylation pathways have been considered, and only the respective lowest energy pathway for each methylation is shown. In H-ZSM-5, the investigated T-12 site is located at the intersection between the straight and the sinusoidal channel. In the transition state of propene elimination, the five-membered ring is oriented in a way that propene leaves the structure along the direction of the straight channel, the barrier for this orientation is found to be 185 kJ/mol. However, we also found another transition state in which the ring is oriented such that propene is eliminated in the direction of the sinusoidal channel. The latter orientation leads to a barrier of only 126 kJ/mol, differing from the first transition state by

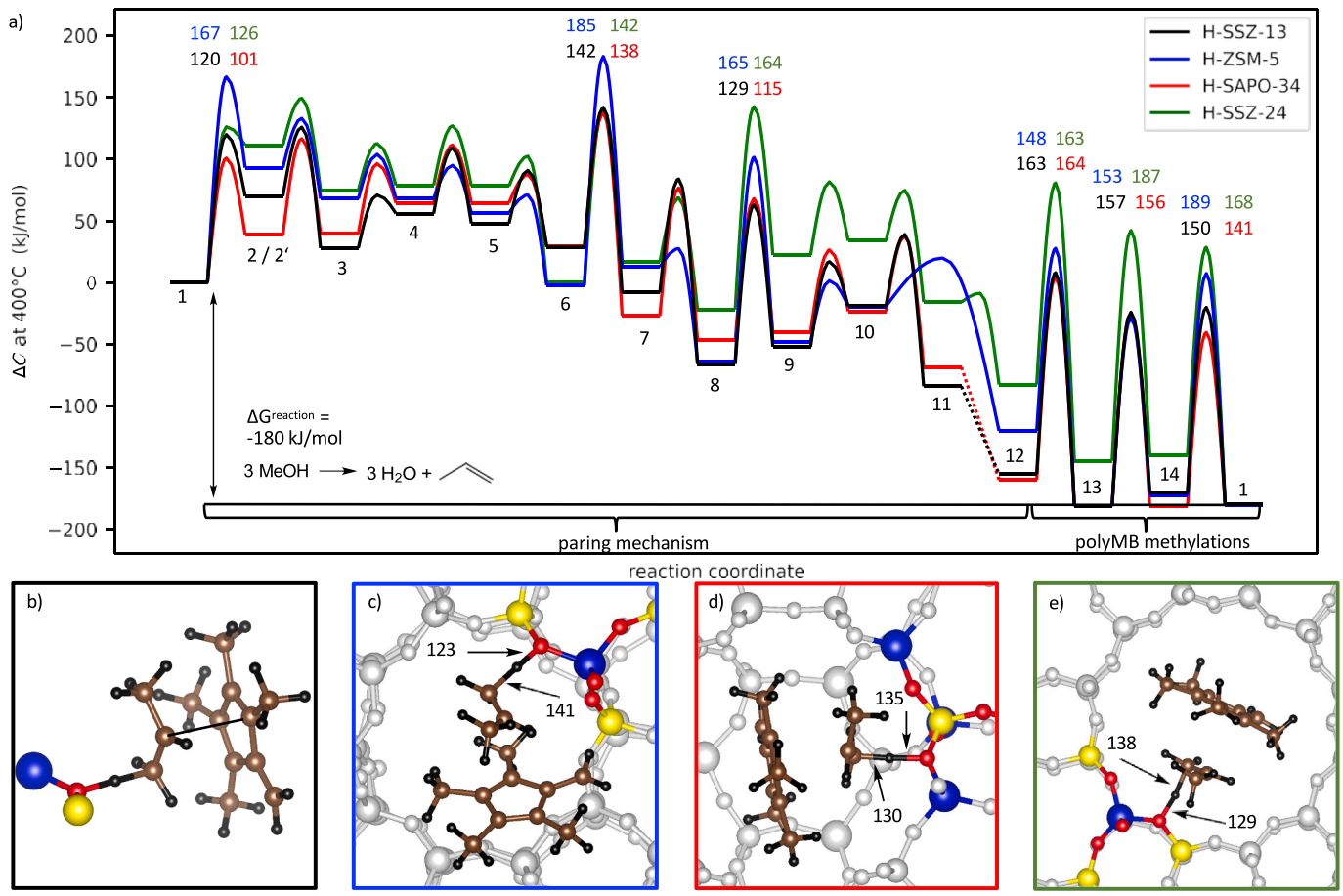

Fig. 2. a) Gibbs free energy diagram of the paring mechanism with propene elimination before ring-expansion (Fig. 1, black cycle) for H-SSZ-13 [31], H-ZSM-5, H-SAPO-34 and H-SSZ-24. Barrier heights are referenced to the lowest preceding intermediate state. This is heptaMB$^+$ (structure 1) for the first barriers, and structure 8 for the ring expansion from 8 to 9. b) Summary of the mechanism showing only the highest free energy barrier, referenced to the lowest preceding intermediate according to the energetic span model. [66] c) Example of the propene elimination transition state (taken from the H-SSZ-24 zeolite), the dashed line indicates the broken C–C bond. d), e) and f) show the propene elimination transition state in the environment of H-ZSM-5, H-SAPO-34 and H-SSZ-24, respectively. For H-ZSM-5, the propene leaves in the direction of the straight channel. Reaction temperature is 400 °C, reference pressure is 1 bar. Bond lengths are indicated in pm. Color code: blue: Al, yellow: Si, red: O, brown: C, black: H. (For interpretation of the references to color in this figure legend, the reader is referred to the web version of this article.)

almost 60 kJ/mol. However, due to the large diameter of heptaMB$^+$, the barriers for rotation of the intermediate in H-ZSM-5 required to connect the most favorable obtained transition states are > 200 kJ/mol. Consequently, we presented in Fig. 1 the most favorable seamlessly connected path. We note that experimental studies in H-ZSM-5 hint towards the fact that not hexaMB, but aromatics with fewer methyl groups are most active in the aromatic cycle. [67–71] However, for simplicity and in order to be able to compare the results of H-ZSM-5 with the other zeotypes we focus on the fully methylated pathway herein. While we restricted our study to hexaMB as the starting point for the comparison of various zeolites, we note that other, less methylated MBs, were shown to have higher reaction barriers by earlier studies. [72] The second-highest barrier for H-ZSM-5 is the deprotonation of heptaMB$^+$ with a barrier of 167 kJ/mol.

H-SAPO-34 is an aluminophosphate with the same CHA structure as zeolite H-SSZ-13, which we investigated in our first study on the paring mechanism. [31] Compared to H-SSZ-13, H-SAPO-34 has a lower acidity [73,74], which would generally be expected to lead to higher transition state energies, because these are generally protonated species. [14,75,76] However, for the aromatic cycle, an uncommon situation arises, in which a cation (heptaMB$^+$) is more stable than the neutral state for most zeolites. Therefore, the lower acidity of H-SAPO-34 mainly results in moving the free energy of hexaMB below that of heptaMB$^+$, thus also changing the most stable reference state, albeit only by 1 kJ/mol. This applies to every neutral intermediate (hexaMB, 2, 7, 10, 12), which are all lower in free energy for H-SAPO-34 than for H-SSZ-13. Overall, the relevant barriers in the paring mechanism are also lower by 1–20 kJ/mol for H-SAPO-34 compared to H-SSZ-13 (see Fig. 2 a)). In a recent study by Ke et al., the revised paring mechanism was integrated in their microkinetic model. [77] The calculated propene elimination barrier in the paring mechanism from the fully methylated five-membered ring in H-SAPO-34 is 144 kJ/mol at the BEEF-vdW level of theory at 0 K [77], which is 6 kJ/mol higher than our respective value at 0 K (138 kJ/mol), and is thus in good agreement.

H-SSZ-24 has a one-dimensional channel structure composed of 12-membered rings, with more space for the substrates than in H-ZSM-5. As opposed to the CHA structure, which consists of cavities, which the aromatics cannot leave through the small windows, the substrate can here diffuse along the direction of the channel. In general, intermediates and transition states are relatively high in free energy, compared to the other zeolites, especially after propene elimination. The highest free energy barrier identified for this zeolite is the ring expansion (TS 8–9) with 164 kJ/mol.

We will now turn to the outcome of the calculations for the second mechanism, where ring-expansion occurs before propene elimination (green path in Fig. 1) which is shown in Fig. 3a)). Starting from structure 5, the ring can directly expand giving structure 6r. After deprotonation of the six-membered ring and protonation of the methylene-group,

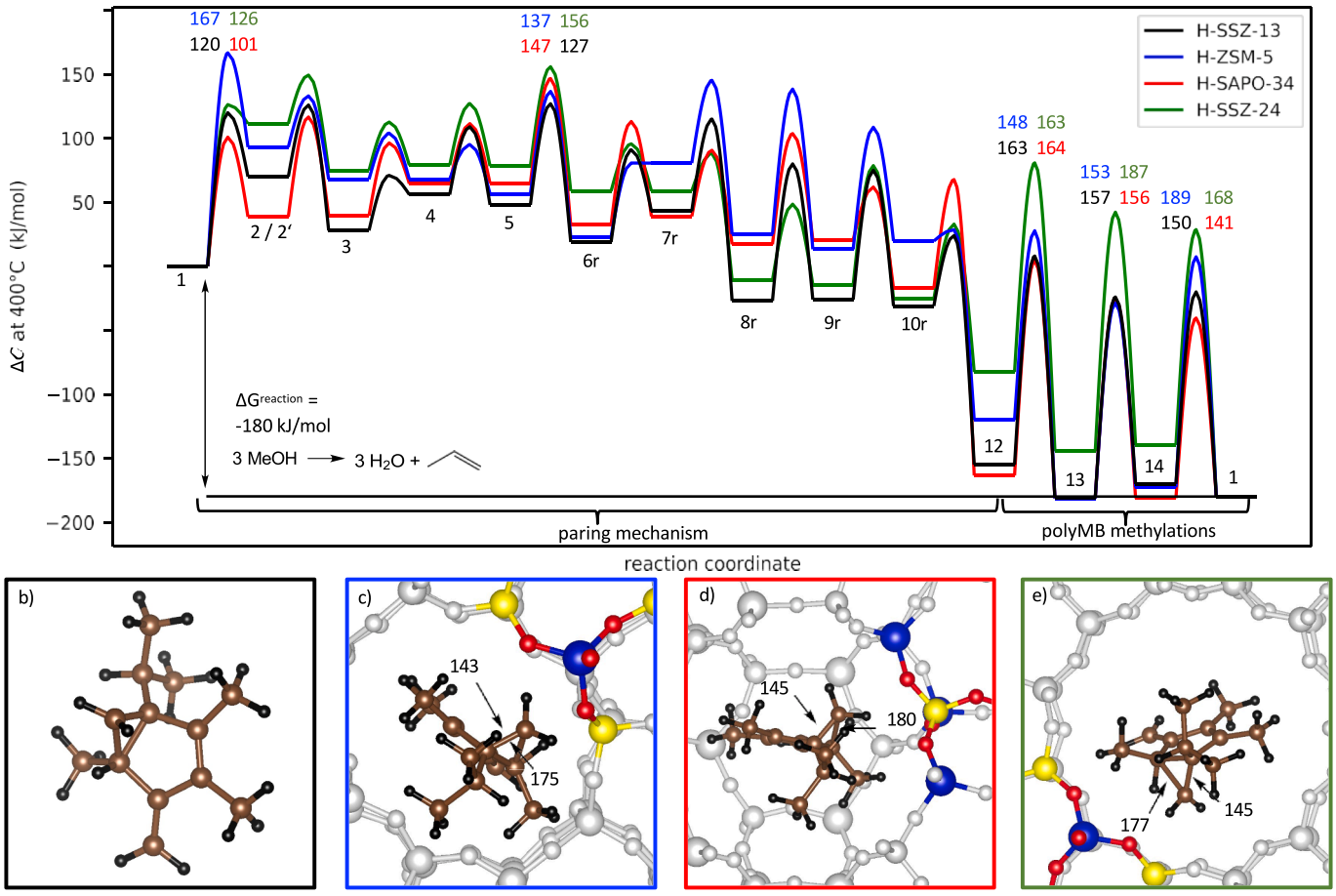

Fig. 3. a) Gibbs free energy diagram of the paring mechanism with ring expansion before propene elimination (Fig. 1, black and green cycle) for H-SSZ-13 [31], H-ZSM-5, H-SAPO-34 and H-SSZ-24. Barrier heights are referenced to the lowest preceding intermediate state, which is structure 1 for H-ZSM-5, H-SSZ-13 and H-SSZ-24 and hexaMB for H-SAPO-34. b) Example of the ring expansion transition state (5 to 6r), taken from the H-ZSM-5 zeolite. c), d) and e) show the ring expansion in the environment of H-ZSM-5, H-SAPO-34 and H-SSZ-24, respectively. Reaction temperature is 400 °C, reference pressure is 1 bar. Bond lengths are indicated in pm. Color code: blue: Al, yellow: Si, red: O, brown: C, black: H. (For interpretation of the references to color in this figure legend, the reader is referred to the web version of this article.)

several methyl-transfer steps lead to structure 10r, in which the propyl- and methylgroup are located at the same carbon atom. From here, propene can also be eliminated, giving tetra-methyl benzene. For H-SAPO-34, H-SSZ-24 and H-SSZ-13, the highest barrier in this reaction is the ring expansion from 5 to 6r. In the study by Ke et al., the apparent energy barrier for this step is calculated to be 107 kJ/mol at 0 K [77] at the BEEF-vdW level of density functional theory and is also the rate-determining step. Their barrier is considerably lower than our barrier at 0 K, which is 135 kJ/mol, which we attribute to the difference in level of electronic structure theory. [47] In H-ZSM-5, deprotonation of heptaMB$^+$ has a barrier of 167 kJ/mol, which is higher in free energy than the ring expansion barrier by 30 kJ/mol, hence constituting the relevant kinetic barrier in this mechanism. The highest barriers in both mechanisms shown in Fig. 1 (the black and green lines) and the highest methylation barriers are compared in Table 1, which contains the summary of the highest reaction barriers for both mechanistic pathways in all four zeolites. The lowest overall barriers for the paring mechanism are found for H-SAPO-34 (139 kJ/mol) and H-SSZ-13 (127 kJ/mol), followed by H-SSZ-24 (156 kJ/mol) and H-ZSM-5 (167 kJ/mol). These are all kinetically feasible at typical MTO temperatures and much lower

Table 1
Free energy barriers in kJ/mol, calculated at 400 °C and a reference pressure of 1 bar computed for the two variants of the paring mechanism (propene elimination first and ring expansion first) and for PMB (polymethylbenzene) methylation and TOFs for the complete mechanism, calculated by using microkinetic modelling and the energetic span model. The paring barriers are given relative two the lowest state within the paring cycle (first row) and with respect to the most stable state including PMB methylation (second row). In cases, where no intermediate within the PMB methylation mechanism is lower in free energy, no additional barrier is given. For PMB methylation, the lowest reference state is generally a minimum within the PMB methylation mechanism, making the analysis simpler. Values for H-SSZ-13 taken from previous paper [31].

Reaction		H-ZSM-5	H-SAPO-34	H-SSZ-24	H-SSZ-13
paring	propene elimination first	6 → TS(6–7) = 185	1 → TS(6–7) = **138**	8 → TS(8–9) = 164	1 → TS(6–7) = 142
		13 → TS(6–7) = 186	14 → TS(6–7) = **139**	–	–
paring	ring expansion first	1 → TS(1-2′) = **167**	1 → TS(5-6r) = 147	1 → TS(5-6r) = **156**	1 → TS(5-6r) = **127**
		13 → TS(1-2′) = **168**	14 → TS(5-6r) = 148	–	–
polyMB methylation		13 → TS(14–1) = 189	12 → TS(12–13) = 164	13 → TS(13–14) = 187	12 → TS(12–13) = 163
TOF	microkinetic modelling	0.13 s^{-1}	1.16 s^{-1}	0.04 s^{-1}	2.97 s^{-1}
	energetic span model	0.03 s^{-1}	2.64 s^{-1}	0.04 s^{-1}	3.15 s^{-1}

than what has been found using the originally proposed paring mechanism where barriers are always well over 200 kJ/mol. [14,15] The methylation barriers, however, have higher free energy barriers than the respective paring mechanism barriers in all zeolites, such that recovering the active hydrocarbon-pool species can be considered the bottleneck in the paring mechanism.

Table 1. also shows the TOFs received with microkinetic modelling and by using the energetic span model. For H-SAPO-34, H-SSZ-24 and H-SSZ-13 they agree very well and the TOFs from microkinetic modelling give slightly lower values than using the energetic span model. For H-ZSM-5, the TOF calculated with the energetic span model is lower than the TOF from microkinetic modelling. This is due to the fact that we use a reference pressure of 1 bar MeOH and no H_2O, i.e. the conditions at the start of the reaction. This makes the methylation barriers irreversible and leads to a higher TOF. In the SI, we also analyzed the microkinetics with additional H_2O pressure.

4. Conclusion

We have investigated a recently identified revised version of the paring mechanism that has been originally proposed for H-SSZ-13. [31] Using DFT and ab initio calculations we found that this mechanism is also viable for the three other zeotypes investigated here (H-SAPO-34, H-ZSM-5 and H-SSZ-24). The highest barriers in this mechanistic pathway are the propene elimination step for H-SAPO-34 (133 kJ/mol), ring expansion for H-SSZ-24 (157 kJ/mol), and hexaMB protonation for H-ZSM-5 (166 kJ/mol). This compares with 265 kJ/mol (ΔE for H-SAPO-34 [14]) and > 240 kJ/mol (ΔG starting from 1,2,3,5-tetramethylbenzene in H-ZSM-5 [15]) that have been found computationally using the original paring mechanism.

Importantly, we thus find that the overall free energy barriers are all kinetically feasible at 400 °C with 133 kJ/mol for H-SAPO-34, 157 kJ/mol for H-SSZ-24 and 166 kJ/mol for H-ZSM-5. Interestingly, the barriers found for H-ZSM-5 are quite a bit higher than in H-SAPO-34 (by almost 40 kJ/mol), which we ascribe to the limited mobility of heptaMB$^+$ in the pore hindering the adsorbate to rearrange and access more favorable transition state structures. The larger pore size of H-SSZ-24 compared to the other zeolites was shown to lead to lower vdW-interactions [37], which results in the generally higher free energy of adsorbed states and the second-highest overall barrier (156 kJ/mol) within the paring mechanism. The higher barriers of H-SAPO-34 compared to the similar H-SSZ-13 (both CHA structure) are due to the lower acidity of H-SAPO-34 [73,74] as discussed above.

In addition to the paring mechanism, we have computed the methylation barriers to recover hexaMB from the tetraMB formed after propene elimination. The barriers for methylation (164 kJ/mol, 187 kJ/mol and 189 kJ/mol for H-SAPO-34, H-SSZ-24 and H-ZSM-5, compared to 163 kJ/mol for H-SSZ-13) are in all cases higher than those within the paring mechanism and are thus predicted to be rate-limiting for the catalytic cycle. The Si/Al ratios of the considered zeolites have been chosen to correspond to one isolated Brønsted site per unit cell. In a recent paper from our group, the effect of a proximate second BAS on the paring mechanism was investigated [72]. In H- SSZ-13, this second site does not actively participate in the reaction mechanism, but increases the reaction barriers indirectly by < 20 kJ/mol, which is in the range also found earlier. [78] Effects can be larger if the second acid site participates in the reaction [72], but we do not expect this in our case. The effect of an additional acid site in CHA zeolites was also investigated by Nystrom et al., who found that a second site affects the acidity of the Brønsted site by changing the deprotonation energy and NH_3-binding energy up to 20 kJ/mol depending on the position of the second site. [79]

Overall, we conclude that the revised paring mechanism is very favorable for the formation of propene in all investigated zeolites giving confidence that propene is indeed mostly originating from the paring mechanism of the aromatic cycle, with overall free energy barriers being around 130–170 kJ/mol, depending on the employed zeotype. This finding can serve as valuable input for kinetic models of this part of the MTO reaction and will lead to a deeper understanding of how selectivity can be tuned and influenced by the catalyst and reaction conditions.

CRediT authorship contribution statement

Annika E. Enss: Data curation, Writing – original draft, Writing – review & editing. **Philipp N. Plessow:** Conceptualization, Data curation, Writing – original draft, Writing – review & editing. **Felix Studt:** Conceptualization, Writing – original draft, Writing – review & editing.

Declaration of competing interest

The authors declare that they have no known competing financial interests or personal relationships that could have appeared to influence the work reported in this paper.

Data availability

All relevant data is provided as SI.

Acknowledgements

The authors acknowledge support by the state of Baden-Württemberg through bwHPC and the German Research Foundation (DFG) through grant no INST 40/575-1 FUGG (JUSTUS 2 cluster) and bwunicluster.

Appendix A. Supplementary data

Supplementary data to this article can be found online at https://doi.org/10.1016/j.jcat.2024.115363.

References

[1] U. Olsbye, S. Svelle, M. Bjørgen, P. Beato, T.V.W. Janssens, F. Joensen, S. Bordiga, K.P. Lillerud, Conversion of methanol to hydrocarbons: How zeolite cavity and pore size controls product selectivity, Angew. Chem. Int. Ed. 51 (24) (2012) 5810–5831.
[2] G.A. Olah, Beyond oil and gas: The methanol economy, Angew. Chem. Int. Ed. 44 (18) (2005) 2636–2639.
[3] G.A. Olah, Towards oil independence through renewable methanol chemistry, Angew. Chem. Int. Ed. 52 (1) (2013) 104–107.
[4] K. Hemelsoet, J. Van der Mynsbrugge, K. De Wispelaere, M. Waroquier, V. Van Speybroeck, Unraveling the reaction mechanisms governing methanol-to-olefins catalysis by theory and experiment, ChemPhysChem 14 (8) (2013) 1526–1545.
[5] I. Yarulina, A.D. Chowdhury, F. Meirer, B.M. Weckhuysen, J. Gascon, Recent trends and fundamental insights in the methanol-to-hydrocarbons process, Nat. Catal. 1 (6) (2018) 398–411.
[6] S. Ilias, A. Bhan, Mechanism of the catalytic conversion of methanol to hydrocarbons, ACS Catal. 3 (1) (2013) 18–31.
[7] D. McCann, D. Lesthaeghe, P. Kletnieks, D. Guenther, M. Hayman, V. VanSpeybroeck, M. Waroquier, J. Haw, A complete catalytic cycle for supramolecular methanol-to-olefins conversion by linking theory with experiment, Angew. Chem. Int. Ed. 47 (28) (2008) 5179–5182.
[8] B. Arstad, S. Kolboe, Methanol-to-hydrocarbons reaction over SAPO-34. Molecules confined in the catalyst cavities at short time on stream, Catal. Letters 71 (3) (2001) 209–212.
[9] B. Arstad, S. Kolboe, The reactivity of molecules trapped within the SAPO-34 cavities in the methanol-to-hydrocarbons reaction, J. Am. Chem. Soc. 123 (33) (2001) 8137–8138.
[10] A. Sassi, M.A. Wildman, H.J. Ahn, P. Prasad, J.B. Nicholas, J.F. Haw, Methylbenzene chemistry on zeolite H-Beta: Multiple insights into methanol-to-olefin catalysis, J. Phys. Chem. B 106 (9) (2002) 2294–2303.
[11] M. Bjørgen, U. Olsbye, S. Svelle, S. Kolboe, Conversion of methanol to hydrocarbons: The reactions of the heptamethylbenzenium cation over zeolite h-beta, Catal. Letters 93 (1) (2004) 37–40.
[12] M. Bjørgen, The methanol-to-hydrocarbons reaction: insight into the reaction mechanism from [12c]benzene and [13c]methanol coreactions over zeolite h-beta, J. Catal. 221 (1) (2004) 1–10.
[13] W. Dai, X. Wang, G. Wu, N. Guan, M. Hunger, L. Li, Methanol-to-olefin conversion on silicoaluminophosphate catalysts: Effect of brønsted acid sites and framework structures, ACS Catal. 1 (4) (2011) 292–299.

[14] C.-M. Wang, Y.-D. Wang, H.-X. Liu, Z.-K. Xie, Z.-P. Liu, Theoretical insight into the minor role of paring mechanism in the methanol-to-olefins conversion within H-SAPO-34 catalyst, Microporous Mesoporous Mater. 158 (2012) 264–271.
[15] C.-M. Wang, Y.-D. Wang, Y.-J. Du, G. Yang, Z.-K. Xie, Computational insights into the reaction mechanism of methanol-to-olefins conversion in h-ZSM-5: nature of hydrocarbon pool, Catal. Sci. Technol. 6 (9) (2016) 3279–3288.
[16] C.-M. Wang, Y.-D. Wang, Y.-J. Du, G. Yang, Z.-K. Xie, Similarities and differences between aromatic-based and olefin-based cycles in H-SAPO- 34 and H-SSZ-13 for methanol-to-olefins conversion: insights from energetic span model, Catal. Sci. Technol. 5 (9) (2015) 4354–4364.
[17] K. De Wispelaere, K. Hemelsoet, M. Waroquier, V. Van Speybroeck, Complete low-barrier side-chain route for olefin formation during methanol conversion in H-SAPO-34, J. Catal. 305 (2013) 76–80.
[18] D. Lesthaeghe, B. De Sterck, V. Van Speybroeck, G. Marin, M. Waroquier, Zeolite shape-selectivity in the gem-methylation of aromatic hydrocarbons, Angew. Chem. Int. Ed. 46 (8) (2007) 1311–1314.
[19] D. Lesthaeghe, A. Horre, M. Waroquier, G. Marin, V. Van Speybroeck, Theoretical insights on methylbenzene side-chain growth in ZSM-5 zeolites for methanol-to-olefin conversion, Chem. Eur. J. 15 (41) (2009) 10803–10808.
[20] S. Wang, Y. Chen, Z. Wei, Z. Qin, H. Ma, M. Dong, J. Li, W. Fan, J. Wang, Polymethylbenzene or alkene cycle? Theoretical study on their contribution to the process of methanol to olefins over h-ZSM-5 zeolite, J. Phys. Chem. C 119 (51) (2015) 28482–28498.
[21] G. Li, E.A. Pidko, The nature and catalytic function of cation sites in zeolites: a computational perspective, ChemCatChem 11 (1) (2019) 134–156.
[22] C. Chizallet, C. Bouchy, K. Larmier, G. Pirngruber, Molecular views on mechanisms of brønsted acid-catalyzed reactions in zeolites, Chem. Rev. 123 (9) (2023) 6107–6196.
[23] I.M. Dahl, S. Kolboe, On the reaction mechanism for propene formation in the MTO reaction over SAPO-34, Catal. Lett. 20 (3) (1993) 329–336.
[24] I. Dahl, S. Kolboe, On the reaction mechanism for hydrocarbon formation from methanol over SAPO-34, J. Catal. 149 (2) (1994) 458–464.
[25] I.M. Dahl, S. Kolboe, On the reaction mechanism for hydrocarbon for- mation from methanol over SAPO-34, J. Catal. 161 (1) (1996) 304–309.
[26] R.F. Sullivan, C.J. Egan, G.E. Langlois, R.P. Sieg, A new reaction that occurs in the hydrocracking of certain aromatic hydrocarbons, J. Am. Chem. Soc. 83 (5) (1961) 1156–1160.
[27] P. Tian, Y. Wei, M. Ye, Z. Liu, Methanol to olefins (MTO): From fundamentals to commercialization, ACS Catal. 5 (3) (2015) 1922–1938.
[28] Y. Chen, S. Wang, Z. Wei, J. Li, M. Dong, Z. Qin, J. Wang, W. Fan, Unraveling the relationship between zeolite structure and MTO product distribution by theoretical study of the reaction mechanism, J. Phys. Chem. C 125 (48) (2021) 26472–26483.
[29] M. Westgård Erichsen, M. Morten, S. Svelle, O. Sekiguchi, E. Uggerud, U. Olsbye, Conclusive evidence for two unimolecular pathways to zeolite-catalyzed de-alkylation of the heptamethylbenzenium cation, ChemCatChem 7 (24) (2015) 4143–4147.
[30] A. Hwang, B.A. Johnson, A. Bhan, Mechanistic study of methylbenzene dealkylation in methanol-to-olefins catalysis on H-SAPO-34, J. Catal. 369 (2019) 86–94.
[31] P.N. Plessow, A.E. Enss, P. Huber, F. Studt, A new mechanistic proposal for the aromatic cycle of the MTO process based on a computational investigation for H-SSZ-13, Catal. Sci. Technol. 12 (11) (2022) 3516–3523.
[32] J.P. Perdew, K. Burke, M. Ernzerhof, Generalized gradient approximation made simple, Phys. Rev. Lett. 77 (18) (1996) 3865–3868.
[33] S. Grimme, J. Antony, S. Ehrlich, H. Krieg, A consistent and accurate ab initio parametrization of density functional dispersion correction (DFT-F) for the 94 elements H-Pu, J. Chem. Phys. 132 (15) (2010) 154104.
[34] G. Kresse, D. Joubert, From ultrasoft pseudopotentials to the projector augmented-wave method, Phys. Rev. B 59 (3) (1999) 1758–1775.
[35] A. Hjorth Larsen, J. Jørgen Mortensen, J. Blomqvist, I.E. Castelli, R. Christensen, M. Dułak, J. Friis, M.N. Groves, B. Hammer, C. Hargus, E.D. Hermes, P.C. Jennings, P. Bjerre Jensen, J. Kermode, J.R. Kitchin, E. Leonhard Kolsbjerg, J. Kubal, K. Kaasbjerg, S. Lysgaard, J. Bergmann Maronsson, T. Maxson, T. Olsen, L. Pastewka, A. Peterson, C. Rostgaard, J. Schiøtz, O. Schutt, M. Strange, K. S. Thygesen, T. Vegge, L. Vilhelmsen, M. Walter, Z. Zeng, K.W. Jacobsen, The atomic simulation environment—a python library for working with atoms, J. Phys.: Condens. Matter 29 (27) (2017) 273002.
[36] P.N. Plessow, F. Studt, Theoretical insights into the effect of the framework on the initiation mechanism of the MTO process, Catal Lett 148 (4) (2018) 1246–1253.
[37] M. Fecık, P.N. Plessow, F. Studt, Influence of confinement on barriers for alkoxide formation in acidic zeolites, ChemCatChem 13 (10) (2021) 2451–2458.
[38] A. Ghorbanpour, J.D. Rimer, L.C. Grabow, Periodic, vdW-corrected density functional theory investigation of the effect of al siting in H-ZSM-5 on chemisorption properties and site-specific acidity, Catalysis Communications 52 (2014) 98–102.
[39] A. Ghorbanpour, J.D. Rimer, L.C. Grabow, Computational assessment of the dominant factors governing the mechanism of methanol dehydration over H-ZSM-5 with heterogeneous aluminum distribution, ACS Catal. 6 (4) (2016) 2287–2298.
[40] A.T. Smith, P.N. Plessow, F. Studt, Effect of aluminum siting in H-ZSM-5 on reaction barriers, J. Phys. Chem. C 125 (37) (2021) 20373–20379.
[41] R.Y. Brogaard, R. Henry, Y. Schuurman, A.J. Medford, P.G. Moses, P. Beato, S. Svelle, J.K. Nørskov, U. Olsbye, Methanol-to-hydrocarbons conversion: The alkene methylation pathway, J. Catal. 314 (2014) 159–169.
[42] R.Y. Brogaard, C.-M. Wang, F. Studt, Methanol–alkene reactions in zeotype acid catalysts: Insights from a descriptor-based approach and microkinetic modeling, ACS Catal. 4 (12) (2014) 4504–4509.
[43] P.N. Plessow, Efficient transition state optimization of periodic structures through automated relaxed potential energy surface scans, J. Chem. Theory Comput. 14 (2) (2018) 981–990.
[44] G. Henkelman, H. Jónsson, Improved tangent estimate in the nudged elastic band method for finding minimum energy paths and saddle points, J. Chem. Phys. 113 (22) (2000) 9978–9985.
[45] G. Henkelman, H. Jonsson, A dimer method for finding saddle points on high dimensional potential surfaces using only first derivatives, J. Chem. Phys. 111 (15) (1999) 7010–7022.
[46] T.J. Goncalves, P.N. Plessow, F. Studt, On the accuracy of density functional theory in zeolite catalysis, ChemCatChem 11 (17) (2019) 4368–4376.
[47] P.N. Plessow, F. Studt, How accurately do approximate density functionals predict trends in acidic zeolite catalysis? J. Phys. Chem. Lett. 11 (11) (2020) 4305–4310.
[48] M. Rybicki, J. Sauer, Ab initio prediction of proton exchange barriers for alkanes at Brønsted sites of zeolite H-MFI, J. Am. Chem. Soc. 140 (51) (2018) 18151–18161.
[49] S. Svelle, C. Tuma, X. Rozanska, T. Kerber, J. Sauer, Quantum chemical modeling of zeolite-catalyzed methylation reactions: Toward chemical accuracy for barriers, J. Am. Chem. Soc. 131 (2) (2009) 816–825.
[50] N. Hansen, T. Kerber, J. Sauer, A.T. Bell, F.J. Keil, Quantum chemical modeling of benzene ethylation over H-ZSM-5 approaching chemical accuracy: A hybrid MP2: DFT study, J. Am. Chem. Soc. 132 (33) (2010) 11525–11538.
[51] J. Sauer, Ab initio calculations for molecule–surface interactions with chemical accuracy, Acc. Chem. Res. 52 (12) (2019) 3502–3510.
[52] M. Fecık, P.N. Plessow, F. Studt, Simple scheme to predict transition-state energies of dehydration reactions in zeolites with relevance to biomass conversion, J. Phys. Chem. C 122 (40) (2018) 23062–23067.
[53] F. Weigend, M. Haser, H. Patzelt, R. Ahlrichs, RI-MP2: optimized auxiliary basis sets and demonstration of efficiency, Chem. Phys. Lett. 294 (1) (1998) 143–152.
[54] D. Feller, Application of systematic sequences of wave functions to the water dimer, J. Chem. Phys. 96 (8) (1992) 6104–6114.
[55] T. Helgaker, W. Klopper, H. Koch, J. Noga, Basis-set convergence of correlated calculations on water, J. Chem. Phys. 106 (23) (1997) 9639–9646.
[56] F. Neese, The ORCA program system, Wires Comput. Mol. Sci. 2 (1) (2012) 73–78.
[57] T.H. Dunning, Gaussian basis sets for use in correlated molecular calculations. i. the atoms boron through neon and hydrogen, J. Chem. Phys. 90 (2) (1989) 1007–1023.
[58] C. Riplinger, B. Sandhoefer, A. Hansen, F. Neese, Natural triple excitations in local coupled cluster calculations with pair natural orbitals, J. Chem. Phys. 139 (13) (2013) 134101.
[59] C. Riplinger, F. Neese, An efficient and near linear scaling pair natural orbital based local coupled cluster method, J. Chem. Phys. 138 (3) (2013) 034106.
[60] C. Riplinger, P. Pinski, U. Becker, E.F. Valeev, F. Neese, Sparse maps—a systematic infrastructure for reduced-scaling electronic structure methods. II. linear scaling domain based pair natural orbital coupled cluster theory, J. Chem. Phys. 144 (2) (2016) 024109.
[61] Y. Minenkov, G. Bistoni, C. Riplinger, A.A. Auer, F. Neese, L. Cavallo, Pair natural orbital and canonical coupled cluster reaction enthalpies involving light to heavy alkali and alkaline earth metals: the importance of sub-valence correlation, Phys. Chem. Chem. Phys. 19 (14) (2017) 9374–9391.
[62] M. Saitow, U. Becker, C. Riplinger, E.F. Valeev, F. Neese, A new near-linear scaling, efficient and accurate, open-shell domain-based local pair natural orbital coupled cluster singles and doubles theory, J. Chem. Phys. 146 (16) (2017) 164105.
[63] F. Neese, F. Wennmohs, A. Hansen, U. Becker, Efficient, approximate and parallel Hartree–Fock and hybrid DFT calculations. a 'chain-of-spheres' algorithm for the Hartree–Fock exchange, Chem. Phys. 356 (1) (2009) 98–109.
[64] O. Deutschmann, S. Tischer, S. Kleditzsch, V. Janardhanan, C. Correa, D. Chatterjee, N. Mladenov, H. Minh, H. Karadeniz, M. Hettel, V. Menon, Detchem, Software package, Version 2.9.1 (2022). URL www.detchem.com.
[65] M. Fecık, P.N. Plessow, F. Studt, A systematic study of methylation from benzene to hexamethylbenzene in H-SSZ-13 using density functional theory and ab initio calculations, ACS Catal. 10 (15) (2020) 8916–8925.
[66] S. Kozuch, S. Shaik, How to conceptualize catalytic cycles? The energetic span model, Acc. Chem. Res. 44 (2) (2011) 101–110.
[67] S. Svelle, U. Olsbye, F. Joensen, M. Bjørgen, Conversion of methanol to alkenes over medium- and large-pore acidic zeolites: Steric manipulation of the reaction intermediates governs the ethene/propene product selectivity, J. Phys. Chem. C 111 (49) (2007) 17981–17984.
[68] M. Bjørgen, F. Joensen, K.-P. Lillerud, U. Olsbye, S. Svelle, The mechanisms of ethene and propene formation from methanol over high silica H-ZSM-5 and H-Beta, Catal. Today 142 (1) (2009) 90–97.
[69] F. Bleken, W. Skistad, K. Barbera, M. Kustova, S. Bordiga, P. Beato, K.P. Lillerud, S. Svelle, U. Olsbye, Conversion of methanol over 10-ring zeolites with differing volumes at channel intersections: comparison of TNU-9, IM-5, ZSM-11 and ZSM-5, Phys. Chem. Chem. Phys. 13 (7) (2011) 2539–2549.
[70] W. Chen, X. Yi, Z. Liu, X. Tang, A. Zheng, Carbocation chemistry confined in zeolites: spectroscopic and theoretical characterizations, Chem. Soc. Rev. 51 (11) (2022) 4337–4385.
[71] C. Li, C. Paris, J. Martınez-Triguero, M. Boronat, M. Moliner, A. Corma, Synthesis of reaction-adapted zeolites as methanol-to-olefins catalysts with mimics of reaction intermediates as organic structure-directing agents, Nat. Catal. 1 (7) (2018) 547–554.
[72] P.N. Plessow, F. Studt, Cooperative effects of active sites in the MTO process: A computational study of the aromatic cycle in H-SSZ-13, ACS Catal. 13 (1) (2023) 624–632.

[73] S. Bordiga, L. Regli, D. Cocina, C. Lamberti, M. Bjørgen, K.P. Lillerud, Assessing the acidity of high silica chabazite H-SSZ-13 by FTIR using CO as molecular probe: Comparison with H-SAPO-34, J. Phys. Chem. B 109 (7) (2005) 2779–2784.
[74] S. Bordiga, L. Regli, C. Lamberti, A. Zecchina, M. Bjørgen, K.P. Lillerud, FTIR adsorption studies of H_{2O} and CH_3OH in the isostructural H-SSZ-13 and H-SAPO-34: Formation of H-bonded adducts and protonated clusters, J. Phys. Chem. B 109 (16) (2005) 7724–7732.
[75] C.-M. Wang, R.Y. Brogaard, B.M. Weckhuysen, J.K. Nørskov, F. Studt, Reactivity descriptor in solid acid catalysis: Predicting turnover frequencies for propene methylation in zeotypes, J. Phys. Chem. Lett. 5 (9) (2014) 1516–1521.
[76] C.-M. Wang, R.Y. Brogaard, Z.-K. Xie, F. Studt, Transition-state scaling relations in zeolite catalysis: influence of framework topology and acid-site reactivity, Catal. Sci. Technol. 5 (5) (2015) 2814–2820.
[77] J. Ke, W.-D. Hu, Y.-J. Du, Y.-D. Wang, C.-M. Wang, Z.-K. Xie, Mi- crokinetic simulations of methanol-to-olefin conversion in H-SAPO-34: Dynamic distribution and evolution of the hydrocarbon pool and implications for catalytic performance, ACS Catal. 13 (13) (2023) 8642–8661.
[78] A.T. Smith, P.N. Plessow, F. Studt, Trends in the reactivity of proximate aluminum sites in H-SSZ-13, J. Phys. Chem. C 125 (30) (2021) 16508–16515.
[79] S. Nystrom, A. Hoffman, D. Hibbitts, Tuning Brønsted acid strength by altering site proximity in CHA framework zeolites, ACS Catal. 8 (9) (2018) 7842–7860.